Talanta 85 (2011) 1672–1679

Contents lists available at ScienceDirect

Talanta

journal homepage: www.elsevier.com/locate/talanta

Acetylsalicylic acid electrochemical sensor based on PATP–AuNPs modified molecularly imprinted polymer film

Zhihua Wang, Hui Li, Jing Chen, Zhonghua Xue, Bowan Wu, Xiaoquan Lu *

Key Laboratory of Bioelectrochemistry & Environmental Analysis of Gansu Province, College of Chemistry & Chemical Engineering, Northwest Normal University, Lanzhou 730070, China

ARTICLE INFO

Article history:
Received 2 April 2011
Received in revised form 27 June 2011
Accepted 27 June 2011
Available online 2 July 2011

Keywords:
Molecularly imprinting
Co-polymerization
Poly-aminothiophenol
Gold nanoparticles
Acetylsalicylic acid

ABSTRACT

A novel electrochemical sensor based on molecularly imprinted polymer film has been developed for aspirin detection. The sensitive film was prepared by co-polymerization of *p*-aminothiophenol (*p*-ATP) and $HAuCl_4$ on the Au electrode surface. First, *p*-ATP was self-assembled on the Au electrode surface by the formation of Au–S bonds. Then, the acetylsalicylic acid (ASA) template was assembled onto the monolayer of *p*-ATP through the hydrogen-bonding interaction between amino group (*p*-ATP) and oxygen (ASA). Finally, a conductive hybrid membrane was fabricated at the surface of Au electrode by the co-polymerization in the mixing solution containing additional *p*-ATP, $HAuCl_4$ and ASA template. Meanwhile, the ASA was spontaneously imprinted into the poly-aminothiophenol gold nanoparticles (PATP–AuNPs) complex film. The amount of imprinted sites at the PATP–AuNPs film significantly increases due to the additional replenishment of ASA templates. With the significant increasing of imprinted sites and doped gold nanoparticles, the sensitivity of the molecular imprinted polymer (MIP) electrode gradually increased. The molecularly imprinted sensor was characterized by electrochemical impedance spectroscopy (EIS), differential pulse voltammetry (DPV), and cyclic voltammetry (CV). The linear relationships between current and logarithmic concentration were obtained in the range from 1 nmol L^{-1} to 0.1 μmol L^{-1} and 0.7 μmol L^{-1} to 0.1 mmol L^{-1}. The detection limit of 0.3 nmol L^{-1} was achieved. This molecularly imprinted sensor for the determination of ASA has high sensitivity, good selectivity and reproducibility, with the testing in some biological fluids also has good selectivity and recovery.

1. Introduction

Acetylsalicylic acid (ASA), commonly known as aspirin, is one of the most important anti-inflammatory drugs in the world. It can be used to relieve minor aches, pains and reduce fever. In recent years, studies show that aspirin is also used to treat the antithrombotic, coronary heart disease, prevent colon cancer and pregnancy induced pre-eclampsy [1,2]. Such widespread use of aspirin has resulted in problems of overdose [3]. To date, various methods have already been proposed to detect ASA and its metabolites such as high-performance liquid chromatography (HPLC) [4–6], ultraviolet spectrophotometry and fluorescence detection [7]. However, some of these instrumental analyses are usually expensive or require sample pretreatment and highly trained technical personnel. Because the ASA has a weak electrochemical activity, there are few reports detecting it through electrochemical methods. Accordingly, it remains a great challenge to develop a rapid, inexpensive but sensitive method for the detection of ASA in biological fluids.

The molecular imprinted polymer (MIP) technique has been demonstrated as one of the most promising techniques in the sensor field [8–12] for its low cost, simplicity, reliability, and wide choice of templates and functional monomers [13–18]. The technique has been widely explored in the field of analytical chemistry, especially in studies on stationary phases for HPLC [19,20], capillary electrochromatography [21], enzyme-linked sorbent for chemiluminescence and colorimetric detection [22]. Owing to the complementarity in binding sites and shape, the created nanocavities can exhibit good selectivity and act as artificial antibodies toward the imprinted molecules, including a large and diverse set of important metal ions [23], organic molecules [24] or bioorganic molecules [25]. The MIP sensor can be divided into four categories according to the origin of signal detection [26,27]: (i) signal due to change in properties of the system as a result of binding of the analyte with the MIP [28,29]; (ii) signal by analyte itself [30–37]; (iii) signal by competitive measurements with displacement [38,39] and (iv) by electrochemical probe [40–42]. Many experiments relating to the molecular imprinted polymer by electropolymerization have been reported [43–46]. As experts agree, the sensitivity of the imprinted sensor was dictated by the amount of effective recognition sites in the molecularly imprinted

* Corresponding author. Tel.: +86 931 7971276; fax: +86 931 7971323.
E-mail address: luxq@nwnu.edu.cn (X. Lu).

0039-9140/$ – see front matter.
doi:10.1016/j.talanta.2011.06.067

polymer films and conductivity. Although the number of the binding sites increases with the increase of the imprinted membrane thickness, thick imprinted membranes can lead to slow diffusion of the analytes to the recognition sites and inefficient communication between the imprinted sites and transducers [47]. To further increase the amount of effective binding sites in the sensor, the simplest method is to provide a higher surface area of the polymer film [48], through the assembly of nanoparticles in the composite membrane [49–51]. In order to improve the conductivity of molecularly imprinted sensor, the most effective way is polymerization of conductive polymers or doping metal nanoparticles. Conclusively, the co-polymerization gold nanoparticles (AuNPs) and conductive polymers of the composite membrane result in high conductivity, large specific surface area, and good biocompatibility [52].

In the present study, we constructed a novel sensor for determination ASA based on MIP and co-polymerized technology. Molecularly imprinted film was modified on the electrode surface, and ASA was linked to the cavities constructed by binding sites of molecularly imprinted film. We hypothesize the combination of surface molecular self-assembly with co-polymerization of poly-aminothiophenol and gold nanoparticles (PATP–AuNPs) on Au electrode will produce the total amount of effective imprinted sites and enhance its conductivity. The molecular imprinting sensor not only strikingly improves the sensitivity and selectivity of ASA analysis, but also obtains good repeatability. Thus, it can be potentially exploited for the detection of ASA and its metabolites in the biological assay. In addition, the sensor can be used to monitor the nonelectrochemical signal substances.

2. Experimental

2.1. Reagents

p-Aminothiophenol (*p*-ATP), Tetrabutylammonium perchlorate (TBAP) and tetrachloroaurate (III) acid ($HAuCl_4$) were purchased from Sigma. Aspirin and salicylic acid were obtained from Aladdin Chemistry Co., Ltd. Benzoic acid and phenol were purchased from Shanghai Chemicals Ltd. Other reagents were commercially available as analytical reagent grade and used without further purification.

2.2. Instrumentation

UV–vis absorption spectra were taken by absorption mode with a UV-1102 UV–vis spectrophotometer (Shanghai, China). The spectra are recorded in the 210–350 nm region. Scanning electron microscopy (SEM) pictures were collected on a Hitachi s-4800 field emission scanning electron microscope (Japan). Cyclic voltammetry (CV) and differential pulse voltammetry (DPV) experiments were performed on CHI-832 working station (CHI instrument, Co. Ltd., Austin, USA). Electrochemical impedance spectroscopy (EIS) experiments were performed on Multi-potentiostat (VMP2, Princeton Applied Research, USA). A three-electrode system consisting of a Ag/AgCl:KCl reference electrode, a platinum wire as counter electrode, and a PATP–AuNPs modified gold electrode (AuE, Φ 3 mm) was used for electrochemical measurements. The impedance spectra were recorded upon the application of the bias potentials in the frequency range 100 mHz to 10 kHz, using an ac voltage of 5 mV amplitude. The data obtained were analyzed using the fitting program in ZSimpWin software. All measurements were carried out at ambient temperature ($18 \pm 2\,^{\circ}C$).

2.3. Pretreatment and self-assembly of Au electrode

A gold electrode was polished with alumina slurry (0.30 and 0.05 μm), rinsed thoroughly with redistilled water, and successively ultrasonicated in ethanol and redistilled water for 5 min. Finally, cyclic voltammetry was performed in 0.5 mol L^{-1} H_2SO_4 solution with the potential range from −0.1 to 1.5 V (scan rate 100 mV s^{-1}). *p*-ATP self-assembly to the surface of Au electrode was carried out by methods that were reported in the literature [47,53,54]. *p*-ATP functionalized electrodes were prepared by immersing the Au electrode into 50 mmol L^{-1} *p*-ATP ethanol solution for 24 h at room temperature, washing the electrode thoroughly with ethanol and double distilled water to remove physically absorbed *p*-ATP. After that, the *p*-ATP modified Au electrode was immersed into an ethanol solution with 1 mmol L^{-1} ASA for 4 h. The electrode was taken out, rinsed with ethanol and double distilled water to remove absorbed ASA, and then dried under nitrogen flow at room temperature.

2.4. Preparation of imprinted PATP–AuNPs–ASA/Au electrode

The *p*-ATP-ASA modified Au electrode was immersed in the ethanol solution containing 10 mmol L^{-1} *p*-ATP, 50 mmol L^{-1} TBAP, 1 mmol L^{-1} ASA and 0.2 g L^{-1} $HAuCl_4$. The co-polymerization was performed by the application of ten cyclic voltammetries in an ice bath with the potential range from −0.3 to 1.2 V (scan rate 50 mV s^{-1}). After the electropolymerization, the composite membrane modified electrode (PATP–AuNPs/Au) was washed in an ethanol: water (4:1) solution containing 0.2 mol L^{-1} HCl in order to remove the ASA template at room temperature for 3 min. Then we rinsed the imprinted PATP–AuNPs/Au electrode with ethanol, double distilled water and finally dried under nitrogen for further use. We prepared a control electrode following the same procedure but without the template molecule. The control electrode was treated by the same procedure as the imprinted electrode to ensure that the effects were observed due only to the imprinting features and not to the subsequent treatments undergone by the electrode.

2.5. Electrochemical measurements

Cyclic voltammetry (CV) measurements are performed in the presence of 10 mmol L^{-1} $[Fe(CN)_6]^{3-}$/$[Fe(CN)_6]^{4-}$ and 0.1 mol L^{-1} KCl solution. Electrochemical impedance spectroscopy (EIS) measurements are recorded upon the application of the bias potentials in the frequency range 100 mHz to 10 kHz, using an ac voltage of 5 mV amplitude. Differential pulse voltammetry (DPV) measurements are performed in the presence of 5 mmol L^{-1} $[Fe(CN)_6]^{3-}$/$[Fe(CN)_6]^{4-}$ and 0.1 mol L^{-1} KCl solution. Above all the measurements were performed at room temperature. Cyclic voltammograms (CVs) of the imprinted membranes were recorded in the potential range of −0.3 to 1.2 V with a scan rate of 50 mV s^{-1} in an ice bath.

2.6. Application of the ASA molecularly imprinted sensor in the biological assay

Four kinds of biological fluids were used to confirm the applicability of this MIP sensor: human plasma, human serum, human saliva, and human urine. Fresh human plasma and human serum were obtained from the local hospital. Human saliva and human urine were harvested from a member of our laboratory. The saliva was collected 15 min after gargling. In order to remove the precipitates, the saliva and urine were centrifuged at 4000 × *g* at room temperature for 15 min. The ASA solutions in biological fluids were prepared by mixing 10 μmol L^{-1} ASA (in ethanol) and 50% biological fluid (in double distilled water) with the ratio of 1:1. The final concentration of ASA was 5 μmol L^{-1} in 25% biological fluids. All the experiment conditions were the same as the foregoing detection.

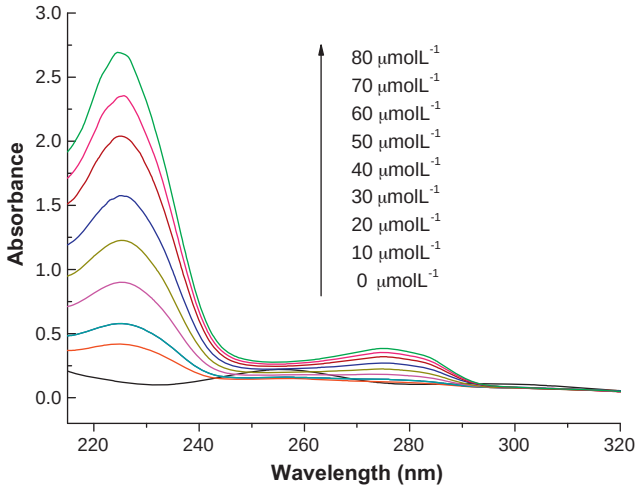

Fig. 1. Evolution of UV spectra with increasing different amounts of ASA into 30 μmol L^{-1} *p*-ATP solution.

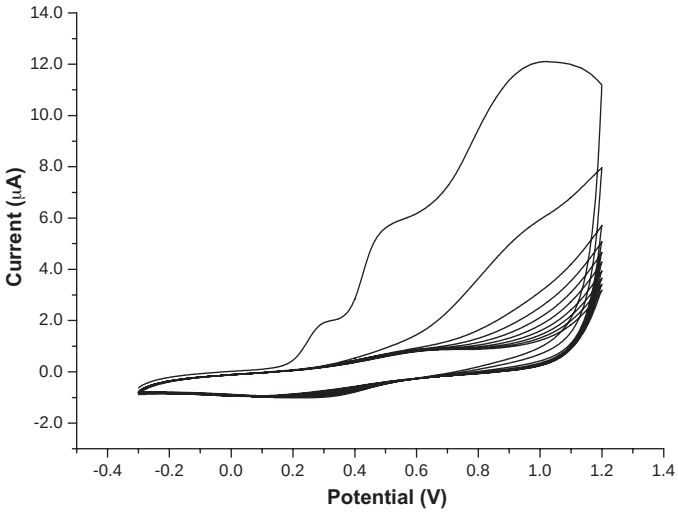

Fig. 2. Cyclic voltammograms for the co-polymerization of 10 mmol L^{-1} *p*-ATP, 0.2 g L^{-1} $HAuCl_4$ and 1 mmol L^{-1} ASA on a gold electrode in ethanol. Scan rate: 50 mV s^{-1}; number of scans: 10; potential range: −0.3 to 1.2 V.

3. Results and discussion

3.1. Preparation of imprinted PATP–AuNPs/Au electrode

Scheme 1A illustrates the preparation procedures of the imprinted PATP–AuNPs/Au electrode. The preparation procedures can be summarized in four steps: Self-assembly *p*-ATP on the surface of Au Electrode; Hydrogen bonding adsorption ASA molecules onto the surface of the ATP modified electrode; co-polymerization of PATP-AuNPs on the surface of ASA/Au electrode; removal of the template ASA molecules from the imprinted PATP–AuNPs membranes. Prior to the co-polymerization, the Au electrode was immersed into *p*-ATP solution for 24 h. A self-assembled monolayer of *p*-ATP molecules was formed on the Au electrode surface by Au–S bonds between gold and the thiol groups (–SH) of *p*-ATP molecules. In the first step of the electrode modification, the *p*-ATP monolayer was chemisorbed on the gold electrode surface and exposed an array of amino groups towards the solution. Secondly, the ATP/Au electrode was immersed into ASA solution for 4 h. ASA molecules in solution phase could be assembled onto the surface of *p*-ATP-modified Au electrode through hydrogen bond interactions between amino groups ($-NH_2$) of *p*-ATP and oxygen atom of ASA (Scheme 1B). The intermolecular interaction between *p*-ATP and ASA could be confirmed by UV absorbance spectra. The maximum absorption wavelength of *p*-ATP shown red shifted in the presence of ASA, and the maximum absorbance of *p*-ATP also increased with the addition of ASA (Fig. 1). These suggest the formation of hydrogen bond interactions between the amino group ($-NH_2$) of *p*-ATP and the oxygen atom of ASA in the solution system. Therefore, the strong hydrogen bond interactions would drive ASA molecules to assemble onto the surface of the *p*-ATP modified electrode. These ASA molecules assembled onto the *p*-ATP modified electrode surface were embedded into the imprinted PATP–AuNPs membranes and formed surface imprinted sites, which would increase the amount of imprinted sites on the electrode surface and enhance the sensitivity of the electrode. Our experiments also reveal that if the incubation step is omitted from the preparation procedures of the imprinted PATP–AuNPs/Au electrode, the DPV responses to ASA would decrease to about 10–15% under the same experimental condition.

Itamar Willner group [46,47,55] have reported the electrodeposition of oligothioaniline AuNPs film using multistep procedures. We improved the one-step co-polymerization method by conducting CV in the 5 mL ethanol solution containing 10 mmol L^{-1} *p*-ATP, 1 mmol L^{-1} ASA and 50 mmol L^{-1} TBAP. Fig. 2 shows the electrochemical process used to form a PATP–AuNPs film on gold electrode. The PATP–AuNPs–ASA film was deposited by repetitively sweeping the potential from −0.3 to 1.2 V (vs Ag/AgCl) at a scan rate of 50 mV s^{-1}. It is observed that an irreversible oxidation process appeared during the first cycle and disappeared during the second cycle. It is well known that Au^{3+} could be easily reduced to Au^0. Therefore, $HAuCl_4$ could be reduced to AuNPs firstly and absorbed on the electrode surface. A oxidation peak was observed at 0.32 V, which indicated that Au^0 is formed on the electrode surface [56]. The reduction peak in 0.29 V may be caused by the AuNPs catalyzing *p*-ATP polymerization. This reduction peak was not occurred, if the $HAuCl_4$ absence in the polymerization of *p*-ATP. An oxidation peak of *p*-ATP was clearly observed at a potential of 0.48 V at the first scan. The results demonstrated that a compact polymeric film was formed and bound to the electrode surface. The decrease of the peak current seems related to the continual formation of PATP–AuNPs composite membranes that leads to the suppression of the voltammetry response. The current gradually reduces with the number of scan circles increasing eventually reaches a steady state. Additionally, the parallel test in the absence of ASA has also been observed. Meanwhile, there is no any difference obtained in the presence/absence of ASA from CVs, indicating that ASA does not exhibit any electrochemical activity in the chosen potential range and its structure is not affected during co-polymerization. Fig. 3 shows the scanning electron micrographs (SEM) of the surface of PATP/AuNPs modified electrodes. The SEM image confirms the formation of AuNPs on the Au electrode surface and the surface of PATP/AuNPs displayed roughness. Moreover, the results indicated that the diameter of the nanoparticles was between 50 and 150 nm.

3.2. Molecular recognition by MIP-modified electrode

The cyclic voltammetry for the MIP film are recorded in 10 mmol L^{-1} $[Fe(CN)_6]^{3-}/[Fe(CN)_6]^{4-}$ solution containing 0.1 mmol L^{-1} KCl, which confirms whether or not ASA has been embedded in the MIP film. During the procedure, $[Fe(CN)_6]^{3-}/[Fe(CN)_6]^{4-}$ was used as the mediator between imprinted electrodes and substrate solutions. Fig. 4 shows the relationship between peak current and surface modification conditions of the gold electrode. For the MIP-Au electrode, the redox peak current decrease rapidly from curve d to a, which can be attributed to the dense film covered the surface of the Au electrode. After the

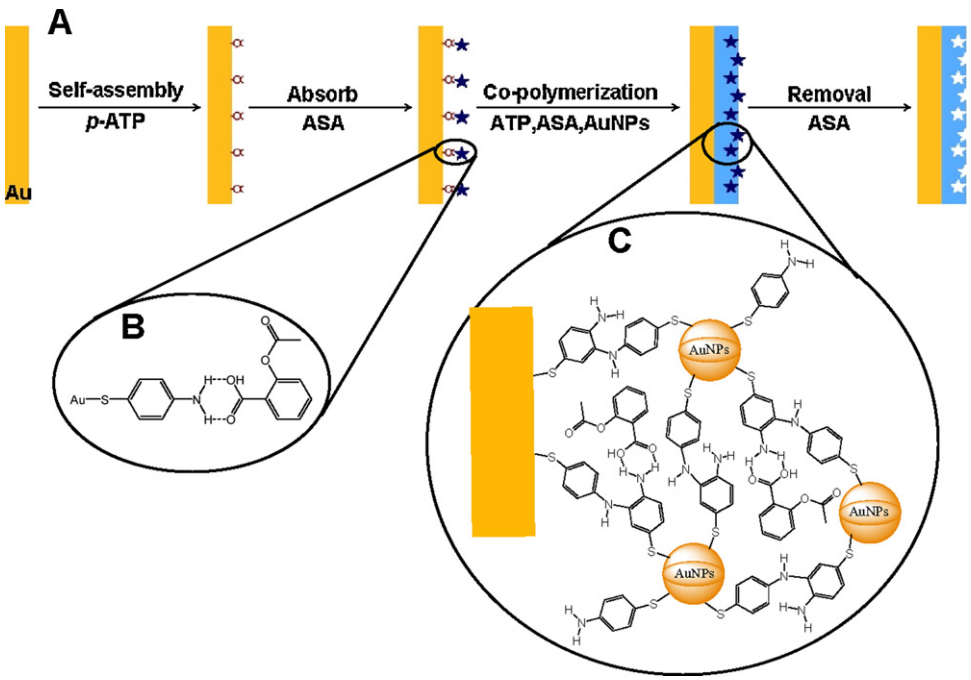

Scheme 1. Scheme of the molecular imprinting technique.

template removal (curve f), a remarkable redox peak is obtained (from curve a to f). The increase of peak current from curve a to f can prove that PATP–AuNPs composite membrane is a kind of conducting film, electro-conductibility better than bare gold electrode. Therefore, the modified electrode has a high sensitivity for detecting ASA. The emergence of curve c can be attributed to the obstruction of the access of $[Fe(CN)_6]^{3-}/[Fe(CN)_6]^{4-}$ through the MIP film after ASA rebinding. This can be explained by the interaction between the ASA and the MIP film, which determines the electron transfer of the $[Fe(CN)_6]^{3-}/[Fe(CN)_6]^{4-}$ ion pair on the electrode surface. In contrast, for the NMIP-Au electrode (curve b), the redox current decreased dramatically from curve d to b, because the PATP–AuNPs film covered the surface of the Au electrode polymerized in the absence of ASA where no cavities with binding sites are obtained. The eluted non-polymerization *p*-ATP in the composite membrane leads to the minor change of redox current, which is negligible after the removal template step. This indicated that the NMIP-Au electrode is unselective and failed to recognize ASA.

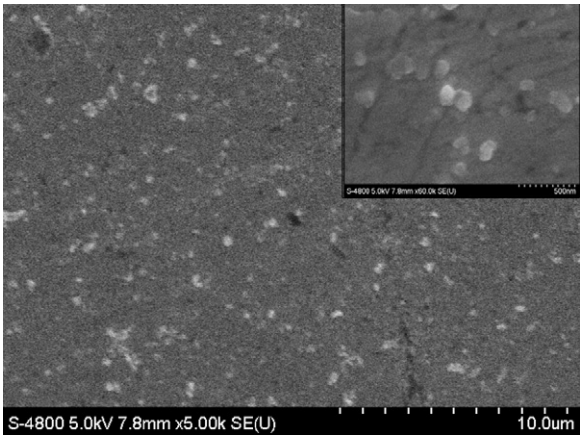

Fig. 3. SEM images of the imprinted PATP–AuNPs membrane formed with ten consecutive potential cycles on the Au electrode surface.

3.3. Electrochemical impedance spectroscopy study of preconcentration time and washing time

It is evident that different preconcentration time and washing time might cause different responses. To determine the optimum operation time for ASA detection, the kinetic experiment has been done. The EIS signal is recorded, and the results are shown in Figs. 5 and 6. Nyquist diagrams (Zim vs Zre) were recorded in 10 mmol L^{-1} $[Fe(CN)_6]^{3-}/[Fe(CN)_6]^{4-}$ containing 0.1 mol L^{-1} KCl as supporting electrolyte. In the electrochemical impedance spectroscopy, a semicircle portion observed at higher frequencies would correspond to the electron-transfer-limited process, a linear section characteristic of the lower frequency is attributable to a diffusion-limited electron transfer. The electron-transfer resistance

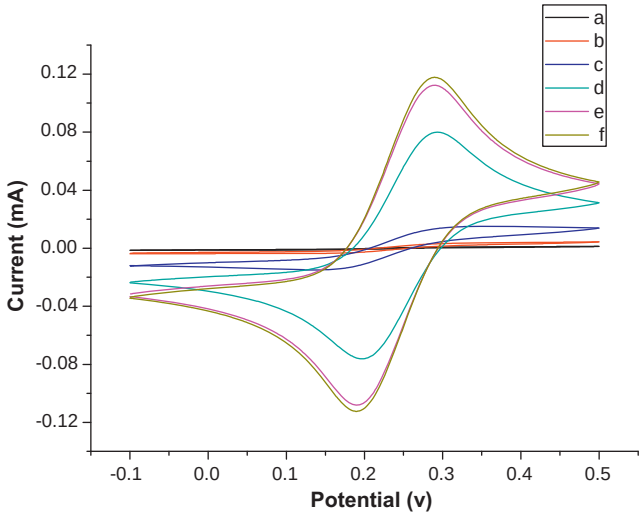

Fig. 4. Cyclic voltammograms of 10 mmol L^{-1} $[Fe(CN)_6]^{3-}/[Fe(CN)_6]^{4-}$ and 0.1 mol L^{-1} KCl at MIP-Au electrode (a), NMIP-Au electrode after template removal (b), MIP-Au electrode after rebinding (c), bare Au electrode (d), MIP-Au electrode after template removal and immersed in the ethanol/water 3 min (e), and MIP-Au electrode after template removal (f). Scan rate: 100 mV s^{-1}.

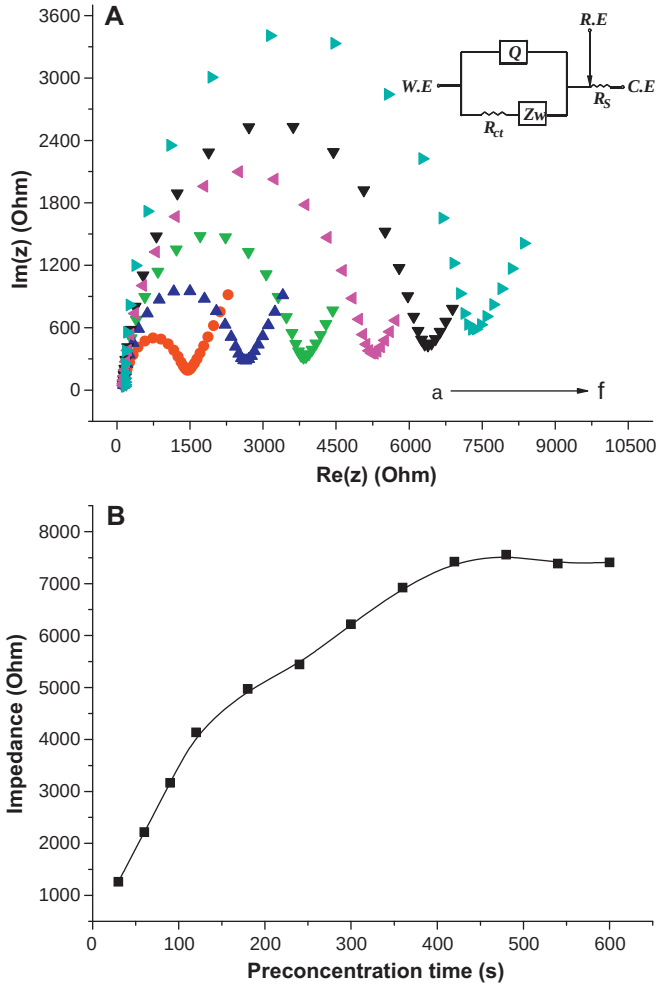

Fig. 5. (A) Impedance spectra corresponding to the PATP–AuNPs/Au electrode immerse in 5 μmol L^{-1} ASA ethanol water solution at different times (the time raised from a to f in turn). The impedance spectra were recorded within the range of 0.1–10,000 Hz at the formal potential of the $[Fe(CN)_6]^{3-}/[Fe(CN)_6]^{4-}$ redox couple. The amplitude of the ac voltage is 5 mV. Inset: the equivalent circuit model used to obtain equations for Zre and Zim. Rs, Rct, Cdl and Zw represent the resistance of electrolyte, the charge transfer resistance, double-layer capacitance and the Warburg impedance, respectively. (B) Impedance response for different times of preconcentration.

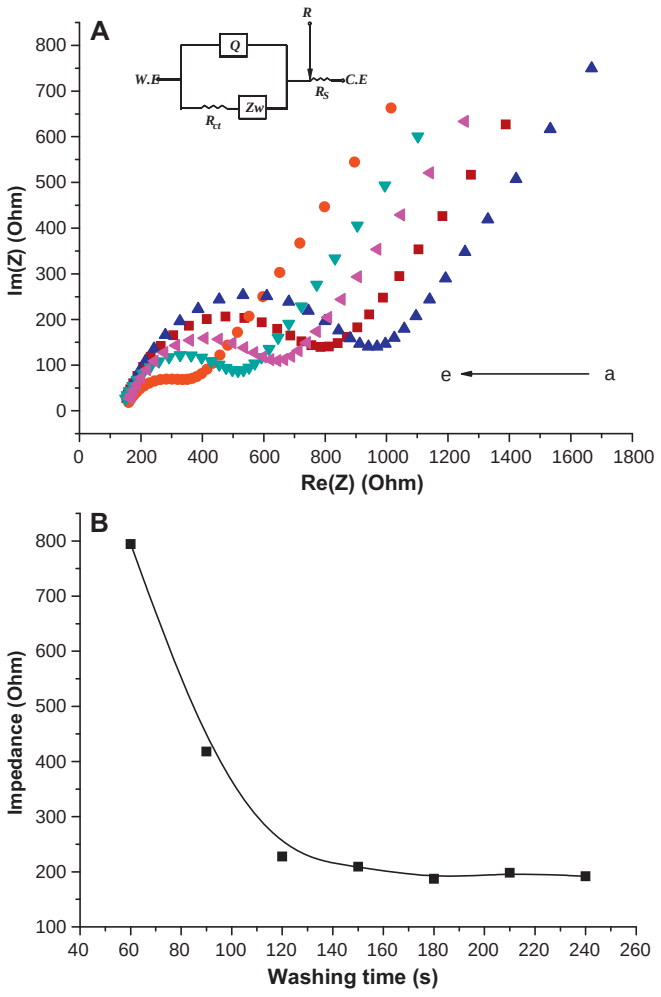

Fig. 6. (A) Impedance spectra corresponding to the ASA–PATP–AuNPs/Au electrode immerse in an ethanol: water (4:1) solution containing 0.2 mol L^{-1} HCl at different times (the time raised from a to e in turn). (B) Impedance response for different times of washing.

(Ret) was indicated by the semicircle diameter, which depends on the dielectric and insulating features at the electrode/electrolyte interface [57].

The preconcentration step is usually a simple and effective way of enhancing the sensitivity of the imprinted sensor [58]. Fig. 5 shows the change of the impedance with the preconcentration time. Because the presence of ASA hinders $[Fe(CN)_6]^{3-}/[Fe(CN)_6]^{4-}$ ion pair's transference on the electrode surface, so different electrochemical impedance diagram can be obtained when the MIP-Au electrode has been preconcentrated in different time with the same concentration of ASA. The impedance increased significantly with the increase of preconcentration time, and a stable response is obtained after 7 min, suggesting that the adsorption equilibrium is reached (Fig. 5(B)). Thus, the preconcentration time of 7 min before the determination of ASA can obtain the strongest electrochemical response. To optimize the washing time, the PATP–AuNPs–ASA/Au electrode was immersed in an ethanol:water (4:1) acid solution, and its stability during washing procedure was investigated by impedance spectroscopy. As shown in Fig. 6, the impedance value gradually decreased and reached minimum at 3 min, remained stable over 3 min. The impedance spectra were recorded within the range of 0.1–10,000 Hz at the bias potential of 0.24 V. The amplitude of the alternate voltage is 5 mV. As a result, the preconcentration time of 7 min and washing time of 3 min were selected for all subsequent assays.

3.4. Electrochemical detection of ASA

For ASA detection, the prepared PATP–AuNPs modified electrode were immersed in different concentrations of ASA solutions (from 1e−10 to 1e−4 mol L^{-1}), and a significant peak current decrease is observed in Fig. 7. It demonstrated that when ASA is rebound, a compact film appears on the surface of electrode again, hindering the electron transfer of the $[Fe(CN)_6]^{3-}/[Fe(CN)_6]^{4-}$ ion pair on the electrode surface. The formed PATP–AuNPs–ASA complex membrane resulted in a decreasing electrochemical reaction of the $[Fe(CN)_6]^{3-}/[Fe(CN)_6]^{4-}$ probe.

In the quantitative analysis, the prepared PATP–AuNPs/Au modified electrode was incubated in different concentrations of ASA for 7 min. Differential pulse voltammograms results of the MIP film were recorded in 5 mmol L^{-1} $[Fe(CN)_6]^{3-}/[Fe(CN)_6]^{4-}$ solution containing 0.1 mol L^{-1} KCl. After a 7 min preconcentration, due to the binding sites in the film occupied by ASA molecules, the peak current decreased with the increase in ASA concentration. As shown in Fig. 8, the decrease of DPV signals were directly related to the concentration of ASA, which is consistent with the CV responses (Fig. 7).

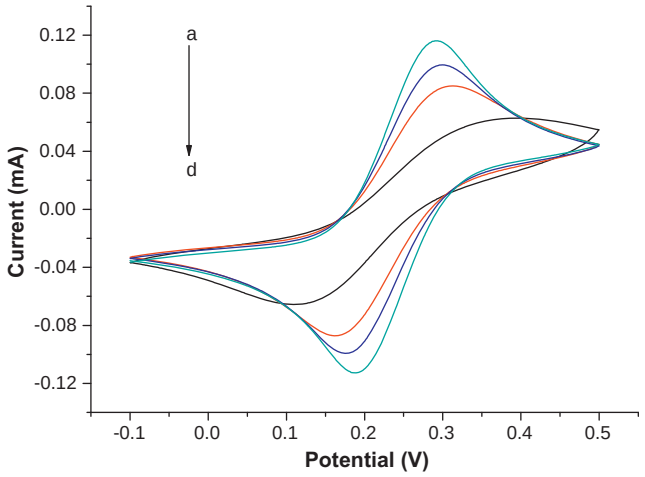

Fig. 7. CV of PATP–AuNPs/Au electrode in 10 mmol L^{-1} $[Fe(CN)_6]^{3-}$/$[Fe(CN)_6]^{4-}$ containing 0.1 mol L^{-1} KCl as supporting electrolyte after incubation in different concentrations of ASA (the concentration could be raised from a to d in turn), Scan rate: 50 mV s^{-1}.

The inset of the Fig. 9, showed there were two linear relationships between current and logarithmic ASA concentration from 1e−9 to 1e−7 (R = −0.99971) and 7e−7 to 1e−4 (R = −0.99448) mol L^{-1}.

There were two different slopes of linear curves, resulting from the different mechanism of molecular recognition in two different ranges of concentration. In the range of 1e−9 to 1e−7 mol L^{-1}, because of the lower levels of ASA in solution, hydrogen adsorption was the main mode of action between the ASA molecular and binding sites. As a result, the large slope of the linear relationship was obtained. However, when the concentration of ASA is higher in the solution, there was a strong Vander Waals force between ASA molecular besides hydrogen bonding adsorption. Thus, the slope of this linear relationship is small. Meanwhile, the lowest detectable concentration, as low as 0.3 nmol L^{-1} is obtained, which is more sensitive than most available ASA detections.

3.5. Selectivity of the molecularly imprinted sensor

An excellent sensor not only possesses good sensitivity, but also has a good selectivity. In order to detect the selectivity of the molecularly imprinted sensor, we chose three kinds of compounds salicylic acid, benzoic acid and carbolic acid for the control experiments, which have a similar structure to ASA. Fig. 10 illustrates different current response signals of the proposed sensing system after the addition of 0.1 mmol L^{-1} salicylic acid, benzoic acid and carbolic acid under the same experimental conditions. It was observed that 10 nmol L^{-1} ASA led to an evident DPV change (Fig. 10(A)). However, when ASA was replaced by 0.1 mmol L^{-1} salicylic acid, 0.1 mmol L^{-1} benzoic acid, and 0.1 mmol L^{-1} carbolic acid, respectively, the MIP-Au electrode hardly showed any change of DPV (Fig. 10(B)–(D)), which proved the ASA molecularly imprinted sensor is highly specific to ASA.

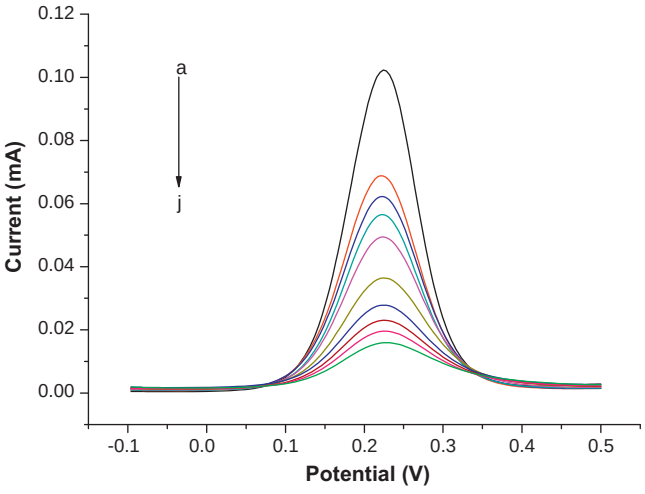

Fig. 8. DPV of PATP–AuNPs/Au electrode in 5 mmol L^{-1} $[Fe(CN)_6]^{3-}$/$[Fe(CN)_6]^{4-}$ containing 0.1 mol L^{-1} KCl. The modified electrode is incubated in different concentrations of ASA: (a-j) 1e−9, 3e−9, 5e−9, 7e−9, 1e−8, 3e−8, 5e−8, 7e−8, 1e−7 mol L^{-1} ASA in ethanol solution for 3 min, respectively.

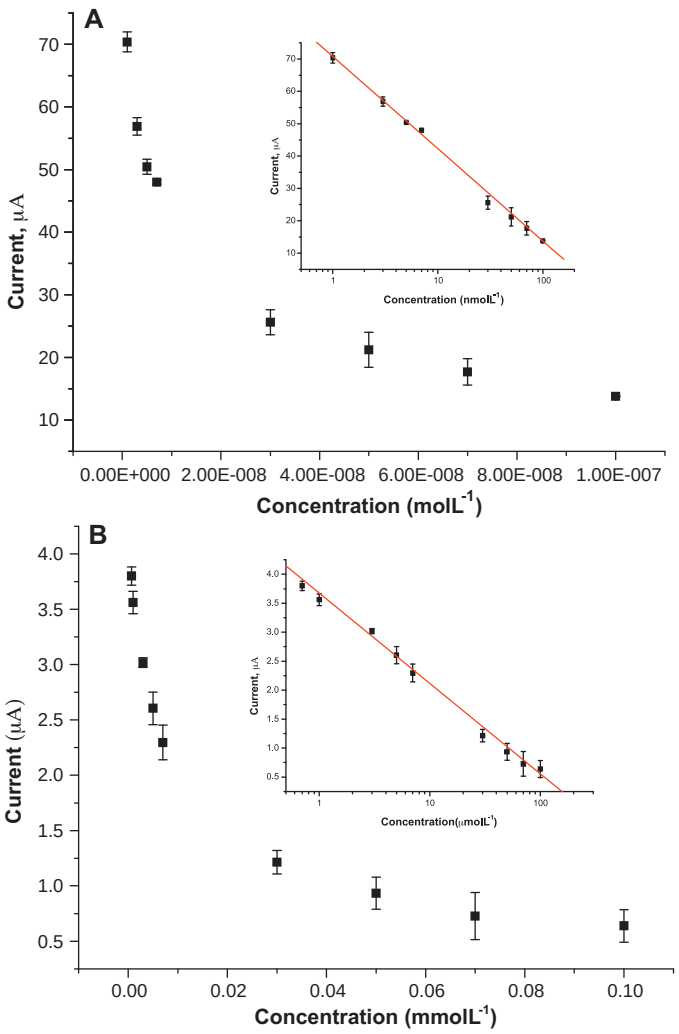

Fig. 9. (A) The relative response of PATP–AuNPs/Au electrode in different concentrations of ASA (from 1 nmol L^{-1} to 0.1 μmol L^{-1}). Inset: A linear detection range is from 1 nmol L^{-1} to 0.1 μnmol L^{-1}. The average of the RSD is 0.0334. (B) The relative response of PATP–AuNPs/Au electrode in different concentrations of ASA (from 0.7 μmol L^{-1} to 0.1 mmol L^{-1}). Inset: A linear detection range is from 0.7 μmol L^{-1} to 0.1 mmol L^{-1}. The average of the RSD is 0.0483.

3.6. Reproducibility and stability of the molecularly imprinted sensor

The reproducibility of the imprinted sensor is estimated by determining the peak current in 5 mmol L^{-1} $[Fe(CN)_6]^{3-}$/$[Fe(CN)_6]^{4-}$ containing 0.1 mmol L^{-1} KCl as supporting electrolyte at room temperature (18 °C) eight times prepared under the same conditions. Prior to detection, immersing the modified electrode in acidic solution of ethanol 3 min remove

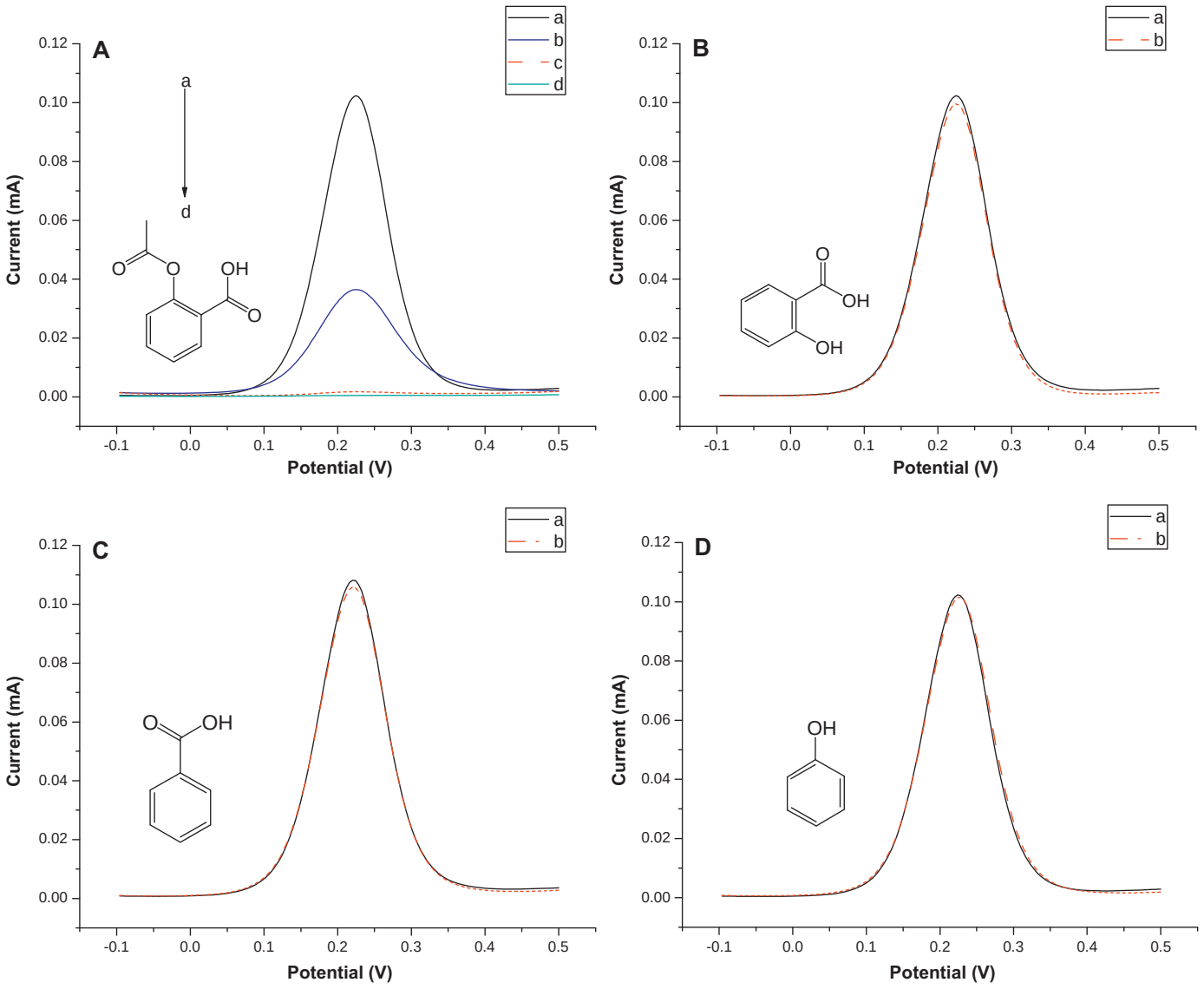

Fig. 10. Selectivity of the molecularly imprinted sensor. ASA (a-d) 0, 1e−8, 1e−4 mol L^{-1} and before removal the template showed an evident decrease in the DPV signal (A), no significant changes of DPV responses for 0.1 mmol L^{-1} salicylic acid (B), 0.1 mmol L^{-1} benzoic acid (C), and 0.1 mmol L^{-1} phenol (D).

template, the following results for the eight times are obtained: 102.80, 98.26, 100.60, 97.63, 99.86, 101.20, 103.70, and 101.10 μA. Relative standard deviation (RSD) of 1.9% was obtained which indicated good reproducibility. The stability of the sensors is an important factor to consider. To ensure stability, the PATP–AuNPs modified Au electrode is stored in the plastic casing with nitrogen at 4 °C over 10 days. It was found that the peak current did not apparently change. After a month, it decreased by about 27%. This indicates that the molecularly imprinted sensor possesses excellent stability.

3.7. Application of the ASA molecularly imprinted sensor in the biological assay

The feasibility of the MIP sensor for practical applications was investigated by analyzing several real samples in comparison with the results of ASA. We chose the human plasma, human serum, human saliva, and human urine as four complex biological fluids. In the 25% biological fluids the same concentration of standard solutions of ASA were detected by DPV measurement. As shown in Table 1, we assessed the ASA detection ability. The MIP sensor to detect ASA was not affected much by ASA in human plasma, human serum and human urine. But the current was obviously increased in human saliva. This may be due to the following facts: human saliva with high viscosity, which cannot completely dissolve in the solution (a group of floc is formed in ethanol water solution) changes the concentration of ASA in the mixture. Except human saliva, the recoveries of this sensor range from 95.7% to 97.1%, and the RSD is less than 3.0%. Total assay time with the proposed procedure is not more than 30 min excluding the purification step. Compared with other methods reported, the major advantage of the method is fast, economical, and simple.

Table 1
Detection of ASA in biologic fluids ($n = 6$).

Biologic fluids	Added (μmol L^{-1})	Found (μmol L^{-1})	Recovery (%)	RSD (%)
25% human plasma	5.000	4.785	95.7	2.68
25% human serum	5.000	4.810	96.2	2.94
25% human saliva	5.000	5.320	106.4	3.41
25% human urine	5.000	4.855	97.1	2.85

4. Conclusions

In this work, a MIP film electrochemical sensor used to indirectly detect aspirin was constructed and first developed co-polymerization of *p*-ATP and $HAuCl_4$ with the cyclic voltammetry in the presence of template ASA molecules. First, ASA molecules hydrogen absorbed to the surface of gold electrode, greatly increased the amount of imprinted sites; then, doped nanoparticles enhanced the sensitivity of MIP sensor. In this measurement the lowest detectable concentration of ASA was 0.3 nM, the linear detection range extended up to 0.7 μM. Furthermore, the fabrication of PATP–AuNPs/Au electrode was very simple and controllable, which facilitates the future design of the integrated electrode according to the different requirements. The results demonstrated that the electrochemical sensor not only could strikingly improve the sensitivity and selectivity of aspirin analysis, but also could obtain good repeatability. Therefore, the electrochemical sensor could be potentially exploited for detecting the overdose of ASA and its metabolites in biological fluids.

Acknowledgements

This work was supported by the National Natural Science Foundation of China (Nos. 20927004, 20965007, 20775060, 20875077, 21005063) and Key Laboratory of Polymer Materials of Gansu Province, China.

References

[1] R.H. Böger, S.M. Bode-Böger, F.M. Gutzki, D. Tsikas, H.P. Weskott, J.C. Frölich, Clin. Sci. 84 (1993) 517–524.
[2] M.F. Attie, J.J.R. Gill, J.L. Stock, A.M. Spiegel, J.R.W. Downs, M.A. Levine, S.J. Marx, J. Clin. Invest. 72 (1983) 676.
[3] T.J. Moore, M.J. Joseph, B.W. Allen, L.A. Coury, Anal. Chem. 67 (1995) 1896–1902.
[4] J.T. Franeta, D. Agbaba, S. Eric, S. Pavkov, M. Aleksic, S. Vladimirov, Il Farmaco 57 (2002) 709–713.
[5] R. Pirola, S.R. Bareggi, G. De Benedittis, J. Chromatogr. B 705 (1998) 309–315.
[6] F. Kees, D. Jehnich, H. Grobecker, J. Chromatogr. B 677 (1996) 172–177.
[7] Z. Bouhsain, S. Garrigues, M.d.l. Guardia, Fresenius J. Anal. Chem. 357 (1997) 973–976.
[8] F.L. Dickert, O. Hayden, K.P. Halikias, Analyst 126 (2001) 766–771.
[9] C. Malitesta, I. Losito, P.G. Zambonin, Anal. Chem. 71 (1999) 1366–1370.
[10] S.A. Piletsky, E. Terpetschnig, H. Andersson, I.A. Nicholls, O.S. Wolfbeis, Fresenius J. Anal. Chem. 364 (1999) 512–516.
[11] J.-M. Lin, M. Yamada, Analyst 126 (2001) 810–815.
[12] D. Kriz, K. Mosbach, Anal. Chim. Acta 300 (1995) 71–75.
[13] C. Xie, B. Liu, Z. Wang, D. Gao, G. Guan, Z. Zhang, Anal. Chem. 80 (2007) 437–443.
[14] D. Gao, Z. Zhang, M. Wu, C. Xie, G. Guan, D. Wang, J. Am. Chem. Soc. 129 (2007) 7859–7866.
[15] K. Haupt, K. Mosbach, Chem. Rev. 100 (2000) 2495–2504.
[16] S. Zimmerman, M. Wendland, N. Rakow, I. Zharov, K. Suslick, Nature 418 (2002) 399–403.
[17] E. Mertz, S.C. Zimmerman, J. Am. Chem. Soc. 125 (2003) 3424–3425.
[18] A. Katz, M.E. Davis, Nature 403 (2000) 286–289.
[19] C. Baggiani, P. Baravalle, G. Giraudi, C. Tozzi, J. Chromatogr. A 1141 (2007) 158–164.
[20] K. Tang, S. Chen, X. Gu, H. Wang, J. Dai, J. Tang, Anal. Chim. Acta 614 (2008) 112–118.
[21] F. Priego-Capote, L. Ye, S. Shakil, S.A. Shamsi, S. Nilsson, Anal. Chem. 80 (2008) 2881–2887.
[22] I. Surugiu, B. Danielsson, L. Ye, K. Mosbach, K. Haupt, Anal. Chem. 73 (2001) 487–491.
[23] G.-Z. Fang, J. Tan, X.-P. Yan, Anal. Chem. 77 (2005) 1734–1739.
[24] B.M. Espinosa-García, W.M. Argüelles-Monal, J. Hernández, L. Félix-Valenzuela, N. Acosta, F.M. Goycoolea, Biomacromolecules 8 (2008) 3355–3364.
[25] X. Kan, Y. Zhao, Z. Geng, Z. Wang, J.-J. Zhu, J. Phys. Chem. C 112 (2008) 4849–4854.
[26] B.J. Privett, J.H. Shin, M.H. Schoenfisch, Anal. Chem. 82 (2010) 4723–4741.
[27] J.r. Heinze, B.A. Frontana-Uribe, S. Ludwigs, Chem. Rev. 110 (2010) 4724–4771.
[28] T.L. Delaney, D. Zimin, M. Rahm, D. Weiss, O.S. Wolfbeis, V.M. Mirsky, Anal. Chem. 79 (2007) 3220–3225.
[29] R. Thoelen, R. Vansweevelt, J. Duchateau, F. Horemans, J. D'Haen, L. Lutsen, D. Vanderzande, M. Ameloot, M. vandeVen, T.J. Cleij, P. Wagner, Biosens. Bioelectron. 23 (2008) 913–918.
[30] H.H. Weetall, K.R. Rogers, Talanta 62 (2004) 329–335.
[31] E. Mazzotta, R.A. Picca, C. Malitesta, S.A. Piletsky, E.V. Piletska, Biosens. Bioelectron. 23 (2008) 1152–1156.
[32] T. Alizadeh, M.R. Ganjali, P. Norouzi, M. Zare, A. Zeraatkar, Talanta 79 (2009) 1197–1203.
[33] J.-L. Gong, F.-C. Gong, G.-M. Zeng, G.-L. Shen, R.-Q. Yu, Talanta 61 (2003) 447–453.
[34] W.-M. Yeh, K.-C. Ho, Anal. Chim. Acta 542 (2005) 76–82.
[35] X. Xu, G. Zhou, H. Li, Q. Liu, S. Zhang, J. Kong, Talanta 78 (2009) 26–32.
[36] C.R.T. Tarley, M.G. Segatelli, L.T. Kubota, Talanta 69 (2006) 259–266.
[37] C.-Y. Huang, M.-J. Syu, Y.-S. Chang, C.-H. Chang, T.-C. Chou, B.-D. Liu, Biosens. Bioelectron. 22 (2007) 1694–1699.
[38] P. Andrea, S.a. Miroslav, S.a. Silvia, M. Stanislav, Sens. Actuators B 76 (2001) 286–294.
[39] S. Kröger, A.P.F. Turner, K. Mosbach, K. Haupt, Anal. Chem. 71 (1999) 3698–3702.
[40] Y. Yoshimi, R. Ohdaira, C. Iiyama, K. Sakai, Sens. Actuators B 73 (2001) 49–53.
[41] V.M. Mirsky, T. Hirsch, S.A. Piletsky, O.S. Wolfbeis, Angew. Chem. Int. Ed. 38 (1999) 1108–1110.
[42] V. Suryanarayanan, C.-T. Wu, K.-C. Hob, Electroanalysis 22 (2010) 1795–1811.
[43] J. Li, F. Jiang, X. Wei, Anal. Chem. 82 (2010) 6074–6078.
[44] C. Xie, H. Li, S. Li, J. Wu, Z. Zhang, Anal. Chem. 82 (2009) 241–249.
[45] L. Özcan, Y. Sahin, Sens. Actuators B 127 (2007) 362–369.
[46] M. Frasconi, R. Tel-Vered, M. Riskin, I. Willner, Anal. Chem. 82 (2010) 2512–2519.
[47] M. Riskin, R. Tel-Vered, T. Bourenko, E. Granot, I. Willner, J. Am. Chem. Soc. 130 (2008) 9726–9733.
[48] J. Du, Y. Wang, X. Zhou, Z. Xue, X. Liu, K. Sun, X. Lu, J. Phys. Chem. C 114 (2010) 14786–14793.
[49] R. Vittal, H. Gomathi, J. Phys. Chem. B 106 (2002) 10135–10143.
[50] F.N. Crespilho, V. Zucolotto, C.M.A. Brett, O.N. Oliveira, F.C. Nart, J. Phys. Chem. B 110 (2006) 17478–17483.
[51] S.S. Kumar, J. Joseph, K.L. Phani, Chem. Mater. 19 (2007) 4722–4730.
[52] S. Xu, X. Han, Biosens. Bioelectron. 19 (2004) 1117–1120.
[53] I. Rubinstein, J. Rishpon, E. Sabatani, A. Redondo, S. Gottesfeld, J. Am. Chem. Soc. 112 (1990) 6135–6136.
[54] Huang, F. Chen, P.A. Bennett, Tao, J. Am. Chem. Soc. 129 (2007) 13225–13231.
[55] M. Riskin, R. Tel-Vered, O. Lioubashevski, I. Willner, J. Am. Chem. Soc. 131 (2009) 7368–7378.
[56] H. Yu, Q.-L. Sheng, L. Li, J.-B. Zheng, J. Electroanal. Chem. 606 (2007) 55–62.
[57] J. Li, J. Zhao, X. Wei, Sens. Actuators B 140 (2009) 663–669.
[58] G. Liu, Y. Lin, Anal. Chem. 77 (2005) 5894–5901.